Earth and Planetary Science Letters 423 (2015) 57–66

Contents lists available at ScienceDirect

Earth and Planetary Science Letters

www.elsevier.com/locate/epsl

Multiple major faults at the Japan Trench: Chemostratigraphy of the plate boundary at IODP Exp. 343: JFAST

Hannah S. Rabinowitz [a,*], Heather M. Savage [a], Terry Plank [a], Pratigya J. Polissar [a], James D. Kirkpatrick [b], Christie D. Rowe [c]

[a] Lamont-Doherty Earth Observatory, Columbia University, Palisades, NY, United States
[b] Dept. of Geosciences, Colorado State University, Fort Collins, CO, United States
[c] Dept. of Earth and Planetary Sciences, McGill University, Montreal, Quebec, Canada

ARTICLE INFO

Article history:
Received 10 December 2014
Received in revised form 6 April 2015
Accepted 7 April 2015
Available online xxxx
Editor: A. Yin

Keywords:
Tohoku earthquake
Pacific plate stratigraphy
shallow subduction structure
ODP Site 1149
DSDP Site 436
IODP Expedition 343

ABSTRACT

We determine the trace element stratigraphy of Site C0019, drilled during the Japan Fast Trench Drilling Project (JFAST) International Ocean Discovery Program (IODP) Expedition 343, to illuminate the structure of the plate boundary following the Tohoku-Oki earthquake of 2011. The stratigraphic units at the JFAST site are compared to undeformed Western Pacific sediments from two reference sites (Ocean Drilling Program (ODP) Site 1149 and Deep Sea Drilling Project (DSDP) Site 436). The trace element fingerprints in these reference sedimentary units can be correlated to individual JFAST samples. At the JFAST site, we find that the accretionary wedge and downgoing plate sediments in the core are composed primarily of Holocene to Eocene sediments. There are several age reversals and gaps within the sequence, consistent with multiple faults in the bottom 15 m of the JFAST core. Our results point to several candidate faults that could have slipped during the 2011 Tohoku-Oki earthquake, in addition to the pelagic clay layer that has been proposed as the main décollement fault.

1. Introduction

The 2011 M_w 9.1 Tohoku-Oki earthquake was a societally devastating event, and was unusual in that peak slip (>50 m) occurred near the seafloor (Fujiwara et al., 2011; Ide et al., 2011; Ito et al., 2011). Although the Tohoku earthquake is the largest earthquake that has been observed in this section of the Japan Trench, tsunami records indicate previous great earthquakes with a recurrence time of approximately 1100 yr (Minoura et al., 2001) and possibly as short as ~500 yr (Sawai et al., 2012; Simons et al., 2011). These large tsunami deposits suggest that the previous great earthquakes may have also caused significant shallow co-seismic slip. Active source seismic surveys indicate that the shallow portion of the accretionary prism at the site of the Tohoku earthquake has experienced significant deformation (Kodaira et al., 2012; Nakamura et al., 2013). Approximately 3 km of displacement has occurred across the plate-boundary at the JFAST site (Chester et al., 2013), and could have resulted from many large earthquakes with shallow slip propagating through the accretionary wedge cored here.

IODP Expedition 343 (JFAST) drilled through the accretionary wedge at the Japan Trench to investigate shallow, tsunamigenic earthquake slip (Chester et al., 2012). Several holes were drilled at the site; one hole was cored (C00019E) and has been studied extensively (Chester et al., 2013; Kirkpatrick et al., 2015; Lin et al., 2014; Rowe et al., 2013; Sawai et al., 2014; Tanikawa et al., 2013; Ujiie et al., 2013; Yang et al., 2013). Samples for this study come from core C00019E, which is hereafter referred to as the "JFAST core". The JFAST core shows many structural features that provide insight into how deformation was accommodated. For instance, there is a change in structural domain with depth. In the top part of the core, above ~820 m below sea floor (mbsf), sediments dip at ~20–80° (Chester et al., 2013; Kirkpatrick et al., 2015) and faults have an average dip of 67° (Chester et al., 2012). At 820 mbsf, a 1-m thick layer of pelagic clay with high smectite content (Kameda et al., 2015) was recovered that showed pervasive shear fabric. Below this layer the bedding has a much shallower dip (~10°; Chester et al., 2013; Kirkpatrick et al., 2015) and there is a change in the anisotropy of magnetic susceptibility (Yang et al., 2013). Temperature measurements at the JFAST site are consistent with the pelagic clay layer accommodating the slip of the Tohoku-Oki earthquake (Fulton et al., 2013; Lin et al., 2014). These observations suggest that the pelagic clay is the boundary between the off-scraped sediments and the

* Corresponding author.
E-mail address: hannahr@ldeo.columbia.edu (H.S. Rabinowitz).

http://dx.doi.org/10.1016/j.epsl.2015.04.010
0012-821X/

subducting material, and has hosted a significant amount of slip, perhaps including the Tohoku earthquake (Chester et al., 2013; Kirkpatrick et al., 2015; Ujiie et al., 2013).

However, multiple faults above and below the pelagic clay layer have been noted and could be important in the slip history of the plate boundary (Chester et al., 2012; Kirkpatrick et al., 2015). It has been difficult to develop a detailed stratigraphy and clear picture of the plate boundary structure at the JFAST site due to significant amounts of missing drillcore (57 m were recovered out of the 831 m drill hole, and there was <50% recovery within the cored sections), lack of reliable strain markers in many observed faults, and the large amount of similar mudstone lithology throughout the JFAST core (Chester et al., 2013, 2012; Kirkpatrick et al., 2015).

Here, we develop a more detailed stratigraphy of the JFAST core based on the trace element chemical compositions of the sediments. Previous studies of the core used a nearby site in the Western Pacific (DSDP Site 436) as a reference site for the incoming plate stratigraphy (Chester et al., 2013; Moore et al., 2015). The correlation between the two ocean drilling sites has been based largely on radiolarian biostratigraphic ages and lithologic characteristics of sediments (Chester et al., 2012). While these age-based methods of correlating stratigraphic units between ocean drill cores are robust for undisturbed Western Pacific stratigraphy (with the exception of the pelagic clays that contain no radiolarians), the sampling for radiolarian analysis in the JFAST core may be too coarse to capture the stratigraphic complexity of the plate boundary. In this paper, we demonstrate a coherent chemostratigraphy in the lithologically equivalent units at Pacific DSDP Site 436 and ODP Site 1149, which allows for a more detailed reconstruction of the stratigraphy of the accretionary wedge at the JFAST site. Our analysis locates intervals of missing section and inverted stratigraphy that indicate the presence of major faults. Some of these faults were previously identified, but their total displacement was unconstrained. Other faults were previously unrecognized in the JFAST core because of the coarseness of radiolarian sampling or because they are within unrecovered sections of the JFAST core. These faults may have accommodated a significant portion of the total displacement along the plate boundary and, therefore, may have accommodated earthquake slip near the trench.

2. Background

Establishing the primary stratigraphic relationships within fault zones is essential to identifying inversions, missing and repeated sections, and other disruptions that can help identify faults. Such data are particularly useful in drillcores where coring gaps and the lack of lateral exposure can obscure important structural features. Sediment ages from biostratigraphy are typically used to date continuously deposited deep ocean sediments that contain flat lying, “layer-cake” units where the law of superposition can be applied as a relative age constraint. However, in tectonically disrupted cores, such as were recovered during the drilling of the accretionary wedge at the JFAST site, it cannot be assumed that the layers have remained in order or intact and superposition does not hold. This creates a challenge in developing a stratigraphy for JFAST sediments. In the JFAST core, radiolarian biostratigraphic data were used to correlate sediments to the nearby DSDP Site 436 site on the incoming plate. While this analysis identified significant structural features, the relatively broad spacing of the biostratigraphic samples increased the likelihood that important stratigraphic offsets were missed.

Here we use trace element analysis to place the JFAST samples within the stratigraphic context of the incoming Western Pacific Plate stratigraphy from the closest available core record in the Japan Trench (DSDP Site 436), corroborated with the more distant core record from Izu–Bonin (ODP Site 1149). Trace element

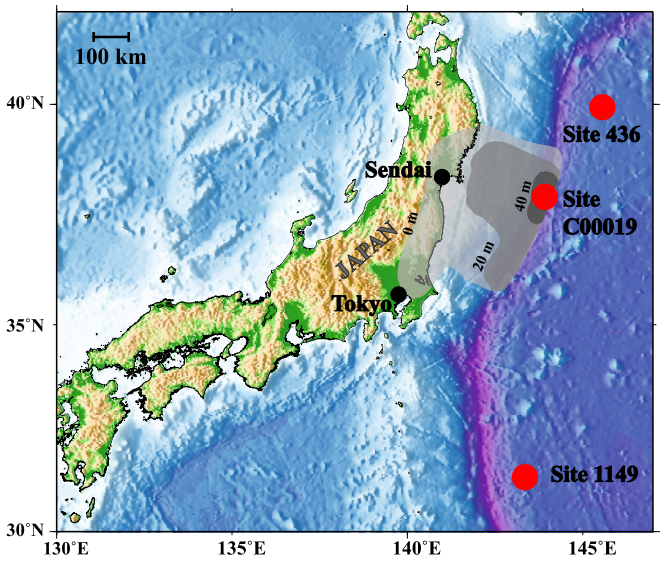

Fig. 1. Bathymetry and topography of the Japan Trench plate boundary. Slip along the plate boundary during the 2011 Tohoku earthquake is shown in gray and contoured in meters (Ammon et al., 2011; Chester et al., 2013; Fujii et al., 2011; Koper et al., 2011). We compare sediments in the JFAST core to stratigraphy at DSDP Site 436 and ODP Site 1149 (labeled red dots). (For interpretation of the references to color in this figure legend, the reader is referred to the web version of this article.)

concentrations in marine sediments are controlled by factors including sedimentation rate, biological productivity in the overlying ocean, and the provenance of sedimentary detritus (Plank and Langmuir, 1998; Plank, 2014). When regions of the Pacific Plate passed through similar depositional regimes concurrently, sedimentary layers with similar ages and similar trace element compositions were deposited (Moore et al., 2015). Therefore, trace elements can be used to develop a geochemical stratigraphy linking widely spaced Pacific Ocean drilling cores. This consistent stratigraphy also indicates that similar lithologies make up the incoming plate at the JFAST site, and that much of the plate boundary stratigraphy consists of disrupted Western Pacific sediments (Chester et al., 2012). Trace element patterns in Western Pacific sediments can therefore be used to correlate the tectonically disrupted stratigraphy of the JFAST site with incoming sediment profiles in nearby cores.

2.1. DSDP Site 436 stratigraphy

DSDP Site 436 is ~200 km NNE of the JFAST site and is comprised of undeformed Western Pacific Plate pelagic sediments (Fig. 1). This site exhibits a 380 m thick, “layer-cake” stratigraphic package from Holocene through Cretaceous sediments (Langseth et al., 1977) (Fig. 2a). The sequence was divided into three units based on age and lithology. Unit 1 is composed of diatomaceous silty clay and claystone and is subdivided into two subunits. Subunit 1A is composed of Holocene to Pliocene greenish vitric (ash-rich) diatomaceous silty clay. Subunit 1B differs gradationally from Subunit 1A in that it shows a higher degree of lithification and is predominantly composed of Late Miocene claystone. There is also a decrease in the average sedimentation rate of Units 1A (~50 m/my) compared with the older Unit 1B (~10 m/my; Table 1). Unit 2 is a darker radiolarian diatomaceous claystone from the Middle to Upper Miocene. The top of Unit 3 is composed of dark brown to nearly black early Miocene to Eocene pelagic clay underlain by Cretaceous chert, sampled as chert cobbles in the two lowermost cores (Langseth et al., 1977). The Miocene/Eocene pelagic clays are devoid of radiolaria but were dated using fish teeth fossils (Doyle and Riedel, 1980). Drilling at DSDP Site 436

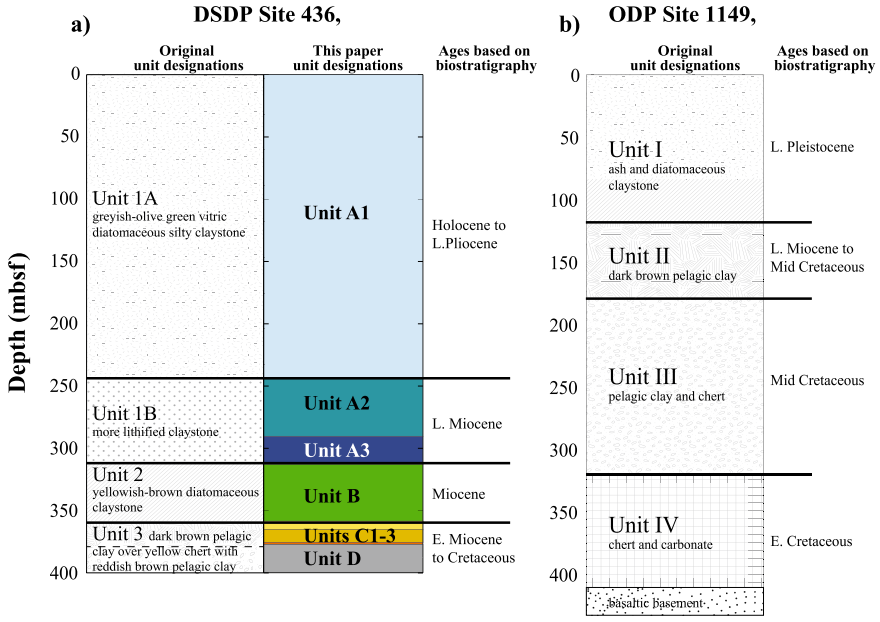

Fig. 2. Stratigraphy and age of Western Pacific reference cores DSDP Site 436 (a, Langseth et al., 1977) and ODP Site 1149 (b, Plank et al., 2000). Both cores show similar stratigraphy with corresponding lithologic units deposited at approximately the same time. The original unit names from DSDP 436 are shown along with the unit names used in this paper (with the unit colors that are also used in Figs. 3–7). (For interpretation of the references to color in this figure, the reader is referred to the web version of this article.)

Table 1
Unit designations for the new chemostratigraphy of the JFAST core. Original DSDP Site 436 unit designations are indicated in addition to the unit designations used in this paper. Unit depths refer to the depths of the incoming stratigraphy at DSDP Site 436. Outlined boxes indicate the most diagnostic trace element indicators for fingerprinting each unit and subunit. Unit D designation is also based on the geochemical characteristics of ODP Site 1149 (Plank et al., 2007).

436-JFAST	Site 436 Unit	Lithological description	age	sed rate m/my	Unit base depths (mbsf)	Cores at DSDP 436	Ce, ppm	Zn, ppm	Co/TiO2	Th, ppm	Ce/Ce*	Zn/Ce
Unit A1	1A	vitric diatomaceous clay	Plio-Pleisto	50	245.5	cores 1-26	< 52	> 86	< 40	< 9	1.1-1.15	>1.7
Unit A2	1B	vitric diatomaceous claystone	Late Mio	10	293	cores 27-31	< 52	< 86	< 40	< 9	1.1-1.15	1.5-1.7
Unit A3	1B	vitric diatomaceous claystone	Late Mio	11	312	cores 31-33	55-70	< 90	< 40	> 9	1.2-1.35	1.3-1.5
Unit B	2	radiolarian diatomaceous claystone	Mid Miocene	12	359.5	cores 34-38	70-100	> 86	35-60	11-14	1.2-1.35	1.1-1.3
Unit C1	3	brown pelagic clay	Early Mio	1	365	core 39	100-125	130 - 150	85-100	14-17	1.4 - 1.5	1.2-1.3
Unit C2	3	brown pelagic clay	Oligocene	1	377	cores 39-40	180-210	150 - 170	250-450	19-22	1.2 - 2.0	<1
Unit C3	3	brown pelagic clay	Eocene	0.1	378	core 40	180-210	170 - 190	< 150	19-22	< 1	<1
Unit D	3	Chert and clay	Late Cret.	-	>397.5	cores 41-42	< 175	< 175	< 135	< 20	<< 1	1-3

ended in the chert layer and did not penetrate to basaltic basement.

2.2. ODP Site 1149 stratigraphy

ODP Site 1149 is located ~1000 km S of the JFAST site (Fig. 1) and ~100 km seaward of the Izu trench. Like DSDP Site 436, this site exhibits a "layer-cake" stratigraphy consisting of similar units (Plank et al., 2000) (Fig. 2b). Unit I is composed of late Miocene to late Pleistocene ash and diatomaceous clay with abundant radiolarians. Unit II contains dark brown pelagic clay that is devoid of radiolarians. Due to the lack of siliceous microfossils, Unit II brown clays were not dated (although they also contain fish teeth), but are constrained to have been deposited between 6.5 and 105 Ma based on biostratigraphic designations within the adjacent units (Bartolini, 2003; Plank et al., 2000). Unit III of ODP Site 1149 exhibits alternating Cretaceous chert and clay layers. Unit IV contains Cretaceous radiolarian chert and chalk (Plank et al., 2000), extending to the Late Valanginian (134 Ma) on top of mid-ocean-ridge type basaltic basement. This carbonate layer is not observed in either of the other cores discussed in this paper (presumably due to the greater age of ODP Site 1149 sediments and basement, variations in local seafloor depth, or lack of penetration past the chert layer in the DSDP Site 436 and JFAST cores).

2.3. Correlation between Sites 436 and 1149

The generalized stratigraphic succession at both DSDP Site 436 and ODP Site 1149, seaward of the Japan and Izu trenches respectively, is identical, with diatom- and ash-rich greenish silty clay overlying dark brown pelagic clay, overlying Cretaceous chert. This succession characterizes most of the western North Pacific, from the Izu, to the Japan, Kurile and Kamchatka trenches (Plank, 2014). The Cretaceous chert was first deposited as biosiliceous ooze when the sites crossed beneath equatorial regions of high productivity. Based on backtracked plate motions, the Western Pacific sites originated in the equatorial Eastern Pacific (Moore et al., 2015). The distinctive brown-to-black, slick pelagic clay, barren of siliceous or carbonate microfossils, was deposited during the northwestward passage of sites beneath the central gyre of the Pacific (Moore et al., 2015). Far from terrestrial sources and in a region of low biological productivity, the sedimentation rate dropped to <1 m/my during this time. At various times in the Miocene (depending upon location) these sites exited the gyre and entered a region of higher biological productivity (as in the modern Kuroshio Current) and entered the Asian dust belt, both factors leading to more rapid accumulation (>10 m/my) of biosiliceous silty clays (Moore et al., 2015). Although this same succession characterizes the Western Pacific trenches from 35–55 °N, the thickness of the units varies latitudinally, with the thickening of the top diatomaceous silty

clays correlated to the thinning of the lower brown clay and chert units from south to north.

2.4. JFAST stratigraphy

IODP Site C0019 is composed of similar lithologies to those discussed above, although the sediments are highly deformed and the original succession disrupted. Due to time constraints, the JFAST expedition sampled 4 discrete depth ranges (176.5–186, 648–660.5, 770–772.35, and 780.5–837 mbsf) and therefore significant sections of the stratigraphy are missing from the core record. The JFAST science party reports seven different sedimentary units, based on lithology and depth. They provide a first-order correlation with the stratigraphy at DSDP Site 436 based on lithology, but are unable to distinguish between lithologically similar units (Chester et al., 2012).

As described in Chester et al. (2012) the first sampled section, 176.5–186 mbsf, is composed of Pliocene green–gray siliceous mudstone (all ages are based on radiolarian dating). The next sampled section, 648–660.5 mbsf, is composed of reddish and bluish, Miocene mudstones. This section is heavily brecciated (possibly during drilling) and could not be used for structural analysis. Below this, between 688.5 and 821.5 mbsf, several mudstone layers are observed, including greenish–brownish–gray, dark gray with black layers, clay-rich, and dark gray pyritic mudstones. These sediments are mostly Pleistocene with the exception of a Pliocene section at 816.5–818 mbsf. From 821.5 to 822.5 mbsf, sediments are predominantly intensely sheared black, scaly clay (with the exception of a less sheared tan mudstone sliver tectonically emplaced within this section). This section of the core has been identified as the décollement (Chester et al., 2013). Surrounding the 1 m-thick recovered pelagic clay layer is about 3 m of unrecovered section (820–821.5 and 822.5–824 mbsf). Therefore, the dark pelagic clay layer has a thickness of <5 m. Below the pelagic clay, there is a yellow– to gray–brown mudstone that overlies orange–pink to buff to dark brown Miocene clays. The final lithology recovered at JFAST is a chert and clay layer beginning at around 831 mbsf (Chester et al., 2012).

Radiolarian ages in the JFAST core are primarily determined from core catcher samples and are taken to be representative of the corresponding core section above (Chester et al., 2012). However, when the number of faults is larger than the number of cores in a segment of the hole, this standard sampling frequency is insufficient to capture multiple age reversals and gaps that could be contained within a single core. Due to the frequency of faulting in the JFAST core, especially close to the plate boundary, it is possible that the ages of the sediments in core catcher samples are not representative of the entire core. It is also probable that several more faults are contained within the unsampled sections at the JFAST site. Furthermore, Pacific radiolarian zones have age ranges that do not always allow for accurate fingerprinting of the sample to the reference core depth. The trace element method described below allows for more precise correlations between the JFAST core and reference cores.

3. Methods

Samples from DSDP Site 436 and JFAST were first extracted with organic solvents for lipid biomarker analyses, and a small amount of the extracted sample ($\sim$1 g) was used for trace element analyses. Digestion and analytical procedures generally follow those in Plank et al. (2007). Sediments were dried at 110 °C before weighing 50 mg into Teflon screw-top vials, to which 3 mL of 8N HNO_3 and 1 mL of HF were added. Samples were digested overnight in sealed capsules on a hot plate ($<$100 °C), then uncapped and evaporated to dryness. Dried samples were re-wetted with DI water and hydrogen peroxide to digest any residual organic matter. Solutions were then acidified with HNO_3, transferred to 250 mL HDPE bottles, diluted with DI water to 3000$\times$ the original dry powder weight, and sonicated for 30 min. A procedural blank as well as standard reference materials (IOBC, IORC, JA-2, W2) were prepared in the same manner with each batch of ten unknowns and analyzed on a PQ ExCell ICP-MS at LDEO. Data were reduced by blank subtraction, external drift correction, and standard calibration. Calibrations were strongly linear ($R^2 > 0.999$), and internal precision based on replicate analyses of each unknown solution is on the order of $<$3% relative standard deviation (RSD). External precision is generally $<$5% RSD for separately digested aliquots of PP829 and IORC (Supplementary Table A). The same solutions were then analyzed on an Agilent 700-series ICP-ES for major elements, except SiO_2, which is volatilized by the HF treatment. Prior tests, however, have demonstrated that SiO_2 can be calculated by difference from a 100 wt% sum within 0.5 wt% absolute (Wade et al., 2005), provided the total volatile content has also been measured by loss on ignition (LOI). Trace elements, major elements, SiO_2-by-difference and LOI concentrations are provided in Supplementary Table A.

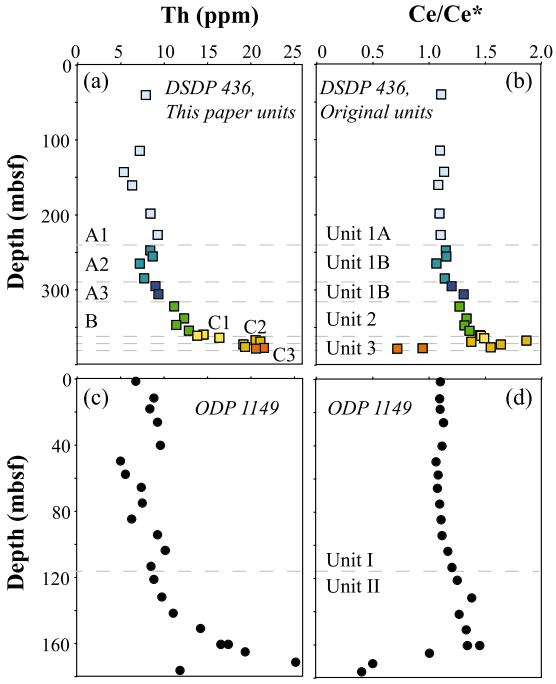

Fig. 3. Key trace element ratios and concentrations demonstrate changing signatures with depth in both reference cores, DSDP Site 436 (a and b) and ODP Site 1149 (c and d). These signatures are consistent across wide ranges of the Western Pacific as seen by the similar signatures in corresponding sedimentary units in both reference cores. Here, we show two examples of trace element signatures – Th (a and c) and Ce/Ce* (b and d). Original DSDP 436 unit designations are shown in b) and unit designation from this paper are shown in a). Site 436 data is color-coded according to the unit colors introduced in Fig. 2. Original ODP 1149 unit designations are shown in d). (For interpretation of the references to color in this figure, the reader is referred to the web version of this article.)

4. Results

4.1. Trace element signatures at DSDP Site 436 and ODP Site 1149

We compared trace element concentrations in the diatomaceous ashy-clay and pelagic clay units above the Cretaceous cherts (at different depths, but similar time horizons at the two sites) for both DSDP Site 436 and ODP Site 1149 (Fig. 3). The concentration of Th increases downcore in both sites, as does the Ce anomaly (Ce/Ce*), which is the deviation of Ce from the adjacent rare earth elements, La and Pr, due to its ability to partially speciate in the

ocean with a different oxidation state (4+ as opposed to the other 3+ REE) (De Baar et al., 1983). Moreover, the absolute values of these tracers in the upper units are nearly identical (5–9 ppm Th and ~1.1 Ce/Ce*) despite the fact that the two sites are >1000 km apart (Fig. 3). At both sites, Th increases dramatically to 20–25 ppm in the brown–black pelagic clay that is barren of microfossils (except fish teeth). The Ce anomaly also increases significantly in the upper pelagic clay before decreasing near the contact with the chert (where it continues to be low, based upon ODP Site 1149 data; Plank et al., 2007). Thorium and Ce/Ce* are both tracers strongly linked to sedimentation rate and the proportion of iron-manganese (FeMn) oxyhydroxides in marine sediments, which form by authigenic precipitation in the water column (Plank and Langmuir, 1998). At low sedimentation rates, FeMn oxyhydroxides predominate as the proportion of detrital and biogenic sediments diminishes to very low values, as occurs in the central gyre of the Pacific. Thorium and Ce^{4+} are both highly particle-reactive, and strongly scavenged by FeMn oxyhydroxides (Anderson et al., 1983; Bau and Koschinsky, 2009). The increases in both tracers downcore reflect the decreasing sedimentation rates as both sites track back to the central gyre. The sharp decrease in Ce/Ce* near the base of the brown pelagic clay (and cherts below) results from higher proportion of fish debris phosphate (which inherits the negative Ce anomaly of seawater; Plank and Langmuir, 1998) and biogenic productivity in general, on the far side of the gyre. Thus, there is a coherent chemostratigraphy at both sites (and indeed much of the Western Pacific; Plank, 2014) that marks the journey through different sedimentation zones across the Pacific.

Although a similar chemostratigraphy characterizes most of the sediments now entering Western Pacific trenches, from the Marianas to the Kuriles, we use the section at DSDP Site 436 as the best template for the original JFAST stratigraphy due to its proximity. The chemical variations at DSDP Site 436 presented here define finer unit boundaries than those originally designated in the initial reports volume (Langseth et al., 1977), and to avoid confusion with the DSDP Site 436 unit boundaries (1–3) and those at ODP Site 1149 (I–IV), we have used different names for the chemostratigraphic boundaries at DSDP Site 436 (Units A–D). DSDP Site 436 Unit 1A corresponds to our Unit A1 and DSDP Site 436 Unit 2 corresponds to our Unit B. We subdivide DSDP Site 436 Unit 1B into two units, Units A2 and A3, and likewise subdivide DSDP Site 436 Unit 3 into four units, Units C1–3 and D (Fig. 2). These subdivisions are notable in that they occur in parts of the core where sedimentation rate decreases downcore. In these locations, the diatom-radiolarian biostratigraphy loses resolution (or ceases to exist entirely) and large chemical gradients form. Thus, the very processes that challenge biostratigraphy improve chemostratigraphy, and the two methods are highly complimentary.

Younger sedimentary units at the reference sites are most difficult to distinguish lithologically and we demonstrate their unique geochemical signatures through several trace element plots (Fig. 4). Classical trace element plots are used to identify sediments with significantly different provenance. However, in the Western Pacific sediments studied here, the units have similar provenance and we use non-standard plots to highlight more subtle differences that can be used to distinguish the subunits. Fig. 4 illustrates the basis for the new chemostratigraphy at DSDP Site 436, and Table 1 provides the criteria for unit designations. Unit C (brown–black pelagic clay) is clearly distinguished from Units A and B by high Th and Ce concentrations, and high Co/TiO_2 (another sedimentation rate proxy), although subunits within Unit C have different proportions of these three tracers (e.g., C3 has intermediate Co/TiO_2). Unit B is also readily distinguished from Unit A based on Th and Ce concentrations, and has a Zn/Ce ratio <1.3. Unit A subdivisions are more subtle and can be most easily identified by variations in Ce and

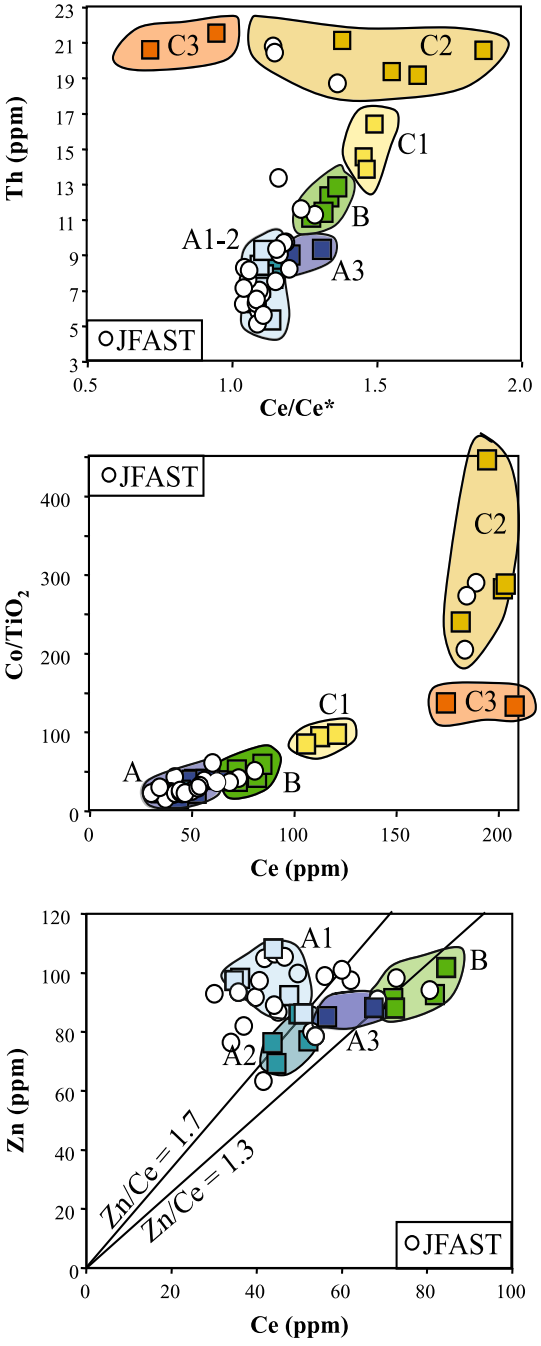

Fig. 4. Scatterplots of key trace element parameters that differentiate between sedimentary units in Western Pacific cores. Colored squares are DSDP Site 436 samples (color-coded by sedimentary unit as introduced in Fig. 2) and white circles are JFAST samples. In these examples, we see that Unit C is distinguishable from Units A and B and can be subdivided into Units C1–3 based on Th, Ce/Ce*, Ce, and Co/TiO_2. Unit B can be distinguished from Unit A based on higher Th and Ce concentrations and lower Zn/Ce (<1.3) values. The bottom plot demonstrates how Unit A can be subdivided into Units A1–3 based on Zn/Ce values as well as higher Ce/Ce* values for Unit A3 than Units A1–2. A more comprehensive list of trace elements used for fingerprinting these sedimentary units can be found in Table 1. (For interpretation of the references to color in this figure, the reader is referred to the web version of this article.)

Zn (Fig. 4). Unit A3 has higher Ce/Ce* (>1.2) than Units A1 or A2; Unit A1 has higher Zn/Ce (>1.7) than Units A2 or A3. Unit A2 occupies an intermediate position in Zn/Ce, with a lower Ce/Ce* than A3 and lower Zn concentration than A1. The Zn/Ce ratio may be a measure of biological productivity, and it is one of the few tracers that varies systematically throughout Unit A. The geochemical dis-

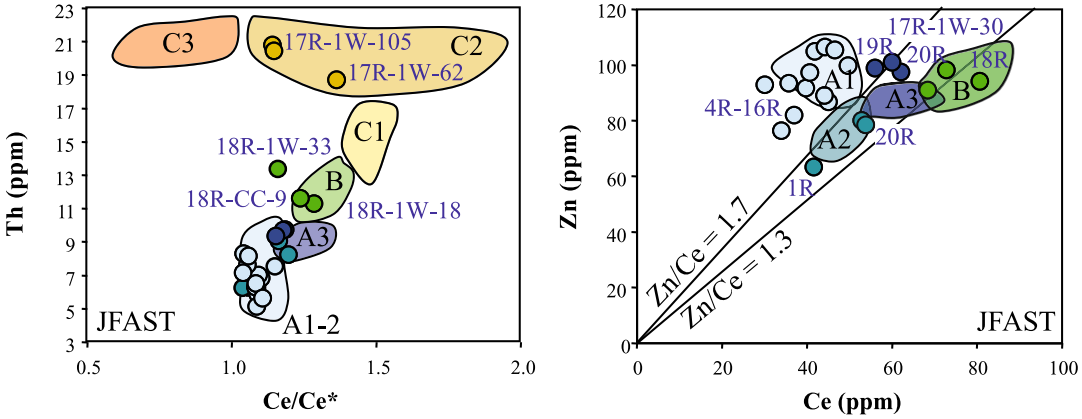

Fig. 5. Assignment of JFAST samples to Western Pacific sedimentary units using the trace element fields from DSDP Site 436 developed in Fig. 4. JFAST samples (circles) are colored according to the sedimentary unit to which they are assigned. Labels indicate core number and depth of the JFAST samples using standard IODP format (core number, tool, section and depth in core). (For interpretation of the references to color in this figure, the reader is referred to the web version of this article.)

tinction between Unit A1 and Unit A2 is more subtle than others that we discuss here, but these subunit designations are consistent with the biostratigraphy. Namely, sediments that are geochemically designated as Unit A1 are late Pliocene to Pleistocene while Unit A2 sediments are Miocene to Pliocene in age. Some of these tracers may be more susceptible to diagenesis or fluid-reactions (Ce/Ce*, Zn/Ce) than others (Th, Ce concentrations and Co/TiO_2). We emphasize that no single tracer, but rather an ensemble of attributes, is diagnostic of any particular subunit (Table 1).

4.2. Trace element signatures at JFAST

We use the above template at DSDP Site 436 to assign JFAST samples to each unit. Fig. 4 shows that the JFAST sediments overlap almost completely with the trace element variations in DSDP Site 436, further supporting a common original chemostratigraphy at both sites. Some of the JFAST sediments have slightly lower Ce/Ce* for the same Th concentration as DSDP Site 436 sediments, and it is possible this is a secondary (diagenetic or fault-fluid reaction) effect due to reduction of Ce^{4+} to Ce^{3+}. Likewise, the Zn concentrations in the youngest JFAST sediments are more varied than those at DSDP Site 436, and this could be due to original or secondary differences in the diatomaceous ashy-clays. We expect Ce and Th concentrations, as well as Co/TiO_2, to be more impervious to secondary processes.

Fig. 5 shows the unit designation for the JFAST sediments, superimposed on the field boundaries defined by DSDP Site 436 sediments. The brown–black pelagic clays of Core 17R clearly correspond to Unit C2. Core 18R sediments are best ascribed to Unit B, while Cores 19R–20R most resemble Unit A2 and A3 sediments, as does Core 1R. The long section of sediment in Cores 4R–16R is assigned to Unit A1. From these designations, it is clear that the stratigraphic sequence is re-ordered in the JFAST core, with older sediments (1R) over younger sediment (4R–16R), and younger sediments (19R–20R) below older sediments (17R).

4.3. Trace element stratigraphy at JFAST

Using the fingerprinted samples from the JFAST core, we present a trace element-based stratigraphy of the subducted Pacific Plate at the JFAST site (Fig. 6). From this analysis, we see that the top of the JFAST core (1R, ~180 mbsf) is composed of Unit A2. This is consistent with radiolarian age dates in this section of the JFAST core of ~4.4 Ma. Below this, there is a large break in core recovery until ~650 mbsf. Based on radiolarian age dating, the top two cores from the second interval of recovery (2R–3R, ~650–660 mbsf) are ~10–11 Ma. Therefore, we assume that these cores can also be designated as Unit A2, although we did not sample this interval for the current study. It is worth noting that because the radiolarian ages of Core 1R are much younger than those of 2R–3R, this could also represent a faulted section. However, with limited core recovery in this shallowest section, no definitive conclusions are possible at this time. From a depth of ~690 mbsf and below, most of the JFAST core is composed of Unit A1, consistent with radiolarian ages of 0.3–3 Ma (Fig. 6). In this section, several faults are described from structural observations of the core. Notably, faults or brecciated regions are observed at ~700, 720, and 817 mbsf (Chester et al., 2013, 2012; Kirkpatrick et al., 2015). All of these faults occur within Unit A1 material where we do not have good chemostratigraphic resolution and cannot identify within-subunit age gaps or inversions.

Near the plate boundary, the structure becomes more complicated and contains several age gaps and inversions. At the identified décollement (17R, ~820 mbsf), Holocene to Late Pliocene Unit A1 overlies the Unit C2 Early Miocene to Eocene pelagic clays. Assuming the Unit A1 samples are from the bottom of the Unit A1 sequence, we give a conservative estimate of ~15 Ma of missing section between the Unit A1 mudstone and Unit C pelagic clays at 820 mbsf. This corresponds with 114 m of missing section assuming unit thicknesses of DSDP Site 436. Within the décollement pelagic clay layer, a mudstone sliver from Unit A3 indicates another significant fault with Unit C2 above and below the sliver. At ~822 mbsf there is a major fault based upon the sharp contacts within Core 17R and the scaly microstructure of the pelagic clay layer that is indicative of shear (Labaume et al., 1997; Moore et al., 1986; Vannucchi et al., 2003).

Below the Unit C2 pelagic clay is Unit B claystone indicating another inversion. Within the Unit B claystone are two faults observed in the JFAST core at 824.4 and 825.1 mbsf (Kirkpatrick et al., 2015), which do not appear in the stratigraphy as inversions or age gaps. Unit B in turn overlies Unit A3. This constitutes another significant age inversion below the pelagic clay, possibly representing a fault within unrecovered section between Cores 18R and 19R. The Unit A3 mudstone overlies an interval of Unit A2 sediment (Fig. 6) at approximately 832 mbsf (Core 20R), another possible stratigraphic inversion. Although no faults have been previously identified at this depth, the inversion of Unit A3 over A2 is marked by a change in mudstone color (with mottling over a distance of ~30 cm) as well as a zone of brecciation. We note here that this sequence of Unit B overlying Unit A3, which, in turn, overlies Unit A2, could represent an overturned section, however, the unit thicknesses are significantly smaller than those at DSDP Site 436. Finally, near the bottom of the JFAST core (within Core 20R) at ~833 mbsf, Unit A2 directly overlies Unit D Cretaceous partially

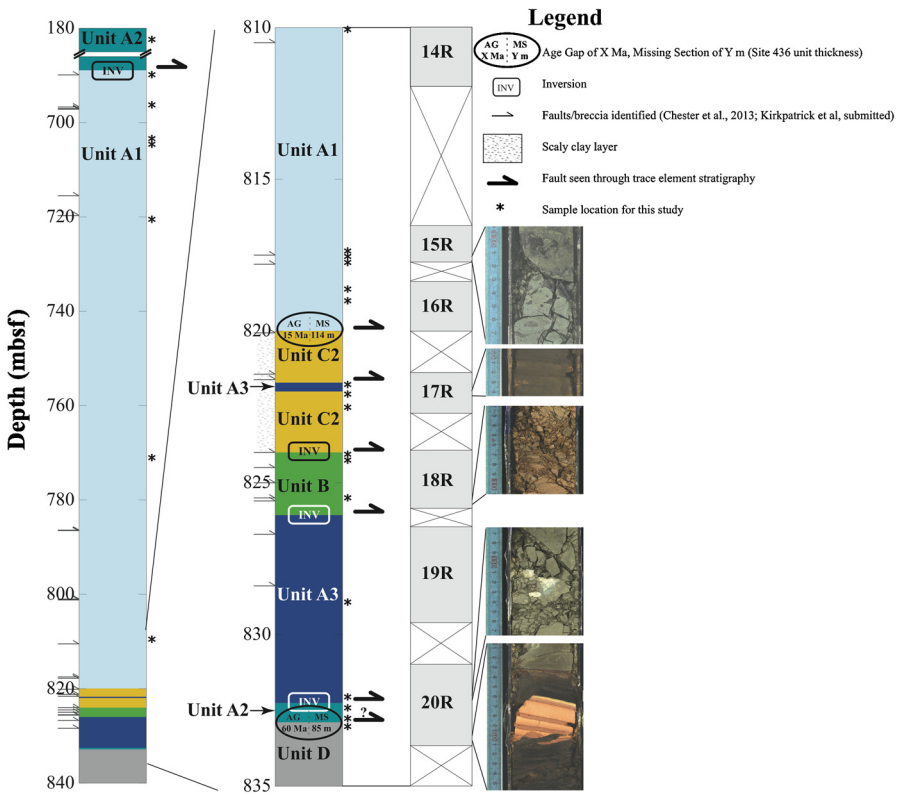

Fig. 6. Stratigraphy of the JFAST site based upon trace element correlations to DSDP 436. Deformation features (i.e. faults, breccia, deformation fabrics) identified in the science party report are indicated with arrows to the left of each stratigraphic column (Chester et al., 2012; Kirkpatrick et al., 2015) and samples from this study are indicated with asterisks on the right. Faults inferred from the trace element stratigraphy are indicated by large arrows to the right of each column. The Japan Trench accretionary wedge at the JFAST site is composed primarily of Unit A material (note the scale break in the left stratigraphic column). There is more stratigraphic complexity approaching the décollement including a significant inversion with Unit C overlaying Units A and B and two age gaps of 15 and 60 Ma, respectively. (For interpretation of references to color in this figure, the reader is referred to the web version of this article.)

silicified clay. This requires a ~60 Ma stratigraphic age gap (~85 m assuming DSDP Site 436 unit thicknesses) above the partially silicified clay layer. This age gap corresponds with deformation features observed in Core 20 such as a dark seam between the Unit A3 mudstone and the finely layered Unit D clay (Fig. 6; Kirkpatrick et al., 2015).

5. Discussion

The trace element approach allows for additional relative age constraints that improve on the stratigraphy at JFAST, especially below the pelagic clay layer. Although several faults were previously identified bounding the pelagic clay layer (Chester et al., 2012; Kirkpatrick et al., 2015), the trace element stratigraphy presented here suggests that several additional large displacement faults exist between the pelagic clay layer at ~822 mbsf and the Cretaceous partially silicified clay at 833 mbsf. These faults are identifiable based on our ability to fingerprint the Quaternary to Miocene mudstones in this interval (Fig. 6). For example, we identify the topmost mudstone in the 824–832 mbsf interval as Unit B. Below this, we see the younger mudstone unit (Unit A3) underlain by Unit A2 mudstone. The stratigraphic inversions present here imply a significant fault at a depth of ~826 mbsf and another at ~832 mbsf. One of the most significant age gaps is observed at ~833 mbsf. Based on trace element measurements, we see Unit A2 material overlying Unit D partially silicified clay. This section is characterized by an extremely thin mm-scale transition from Unit A mudstone to Unit D partially silicified clay. The presence of a potential gouge layer (see core images in Fig. 6) as well as slight misorientation of bedding in the pelagic clay below this contact suggest that the ~60 Ma of missing stratigraphy here could imply a major fault.

Notably, the bedding below Core 17R is much more shallowly dipping (~10° rather than ~67° above the pelagic clay layer). The absence of observed bedding cutoffs in the deeper JFAST cores suggests that any faults in this section are sub-parallel to bedding and likely highly localized. The localized shear strain accommodated by the faults would not have been captured by the anisotropy of magnetic susceptibility (AMS) results (due to sample spacing), which suggest vertical shortening in the deeper part of the section (Yang et al., 2013). It follows that even though the faults we document would have accommodated little flattening, our observations are not inconsistent with the AMS results. Significant amounts of displacement would be required to explain the stratigraphic reversals and gaps on low dip structures. This may imply that the dip is not regionally constant on individual fault strands, consistent with a duplex or fault ramp model (Fig. 7).

Chester et al. (2013) estimated that the plate boundary at the JFAST site has hosted ~3.2 km of displacement based on balancing a two-dimensional cross-section. Because the pelagic clay layer showed the most pervasive deformation, the largest age gap in the biostratigraphy, and a low frictional strength at both slow and fast velocities (Ikari et al., 2015; Ujiie et al., 2013), most of the 3.2 km of displacement was thought to occur within it. We have shown here that the faults we identify at the JFAST site may have accommodated a significant amount of the inferred plate boundary slip, implying that cumulative displacement at the plate boundary was not localized exclusively in the pelagic clay layer but rather distributed among several major faults. Adding together the faults inferred from the chemostratigraphy, along with the distances between them (cf. Rowe et al., 2013) yields a plate boundary thickness ~15 m which is consistent with the maximum décollement thickness proposed by Kirkpatrick et al. (2015). We also note that

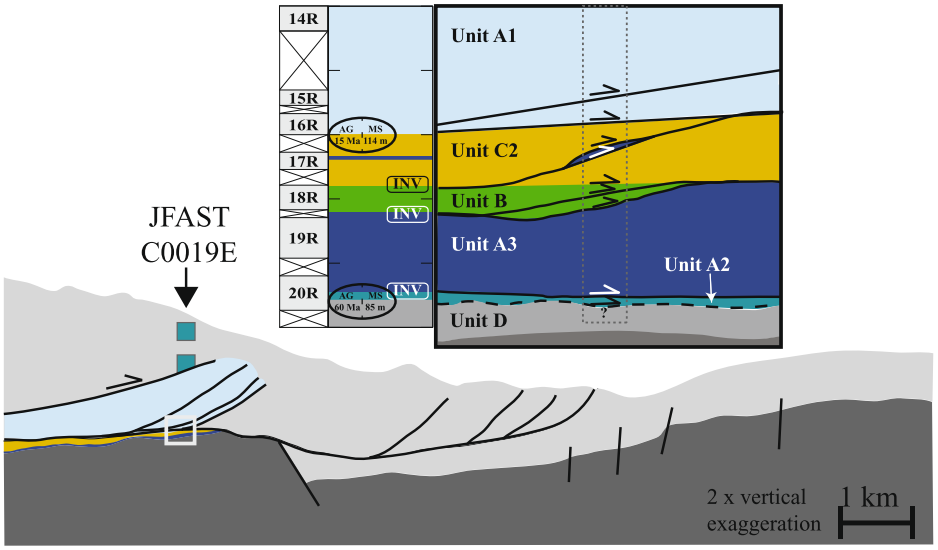

Fig. 7. Structural interpretation of the accretionary wedge in the Japan Trench based on our trace element stratigraphy at Site C0019E. Light gray sediments in the accretionary wedge are undifferentiated frontal prism sediments that are unconstrained by our data. Dark gray at the bottom is basement. Inset is a blow-up of the region boxed in white from the larger cross section. The stratigraphic section developed in this paper and the core recovery are shown to the left of the blow-up. The section inferred to have been drilled at JFAST is indicated by the dark gray dotted line in the structure blow-up. After Kirkpatrick et al. (2015). (For interpretation of references to color in this figure, the reader is referred to the web version of this article.)

because the JFAST core did not penetrate to basement, significant faults could have been missed below the bottom of the recovered JFAST section. A thicker décollement (at least 10 m) would be more in keeping with observations in other subduction zone settings such as Barbados (Maltman et al., 1997), although estimates from Nankai suggest a décollement more on the order of tens to hundreds of meters (Moore et al., 1990; Rowe et al., 2013; Ujiie and Kimura, 2014). Our results imply that structures with insignificant appearance in the core, such as thin shear surfaces with little notable damage surrounding them, may be responsible for significant displacement.

The pelagic clay layer in the JFAST core, like most smectite-rich clays, is frictionally weak and extremely velocity weakening at high slip rates, indicating that both aseismic and seismic slip could occur within this layer (Faulkner et al., 2011; Ikari et al., 2015; Sawai et al., 2014; Ujiie et al., 2013). However, the presence of multiple, large-displacement faults in the surrounding sediments implies that shallow slip was not exclusively localized within the pelagic clay. This could suggest that the path of a rupture during dynamic seismic slip might not be completely controlled by differences in friction between stratigraphic units. Instead, earthquake rupture might propagate or branch in a more chaotic way (Poliakov et al., 2002). Furthermore, low velocity friction experiments on samples from the JFAST core show that the younger mudstones, though frictionally stronger than the pelagic clay, are significantly more velocity weakening (Ikari et al., 2015).

While we can determine that significant displacement took place on a fault by noting major stratigraphic inversions and age gaps, we cannot tell which earthquake, how many earthquakes, or even if an earthquake rather than aseismic creep was responsible for the displacement based on the chemostratigraphy presented here. Although the stratigraphy suggests large displacement, it does not require any particular inversion or age gap to have been produced specifically by the Tohoku earthquake. Nonetheless, the depth range over which significant faults are identified is not excluded by temperature data collected from a thermistor string installed during the JFAST project (Fulton et al., 2013). Inversions of the temperature data are consistent with a fault that was frictionally heated during the earthquake, and several of the faults identified in the JFAST core could fit the slip location identified in the temperature data.

There are a number of additional factors that might affect the trace element method of identifying stratigraphic units, including overlapping elemental fingerprints, sediment mixing, fault heating and fluid flow. Western Pacific units in this study can be distinguished using multiple trace element signatures, however this could be an issue in other regions. Mixing of multiple units could occur if a sample is collected on a border between different units or as a result of faulting if there is soft-sediment deformation during an earthquake. Mixing would cause the sample to exhibit trace element signatures intermediate between the two homogenized units. While we do observe some JFAST samples that fall outside of the trace-element fields defined from DSDP Site 436, they are generally not along tie lines between fields, suggesting mixing is minimal. Bedding is also evident in non-faulted regions indicating mixing is unlikely to be an issue for many of the samples. Finally, we have not explicitly considered the role of fault heating or faulting-related fluid flow to mobilize certain elements (Ishikawa et al., 2008) and, thus, change the trace element signature in the JFAST core relative to that of the corresponding stratigraphic unit in the reference cores. While Zn concentrations and Ce/Ce* could potentially be altered by this process, Ce and Th concentrations and Co/TiO_2 ratios that are also used to define the chemostratigraphy should be less susceptible to these processes.

6. Conclusions

Based on trace element geochemistry, we fingerprint stratigraphic units in the Western Pacific to develop a detailed stratigraphy of the JFAST core. The trace element stratigraphy agrees well with the coarse stratigraphy determined by radiolarian age dating, while also identifying several age inversions and sections of missing stratigraphy that were not apparent from the biostratigraphy. These features require multiple faults within a ~15 m-thick zone of sediment above the Cretaceous chert layer at the bottom of the JFAST core. Our findings imply that deformation at the plate boundary was not limited to the frictionally weak pelagic clay layer as previously suggested. Rather, the large displacement faults iden-

tified here should be considered as candidate faults for the Tohoku earthquake.

Acknowledgements

Samples for this study were provided by the International Ocean Discovery Program (IODP). We thank the curatorial staff at the Kochi Core Center for help obtaining samples. Funding for this project was provided by U.S. National Science Foundation grant OCE 12-60555 and a Schlanger Ocean Drilling Fellowship to H.S.R., part of the NSF-sponsored U.S. Science Support Program for IODP that is administered by the Consortium for Ocean Leadership, Inc. Thanks to Siobhan Campbell for work in processing samples for trace element analysis. We thank editor An Yin and an anonymous reviewer for helpful suggestions on the manuscript.

Appendix A. Supplementary material

Supplementary material related to this article can be found online at http://dx.doi.org/10.1016/j.epsl.2015.04.010.

References

Ammon, C.J., Lay, T., Kanamori, H., Cleveland, M., 2011. A rupture model of the 2011 off the Pacific coast of Tohoku Earthquake. Earth Planets Space 63, 693–696.

Anderson, R.F., Bacon, M.P., Brewer, P.G., 1983. Removal of ^{230}Th and ^{231}Pa at ocean margins. Earth Planet. Sci. Lett. 66, 73–90.

Bartolini, A., 2003. Cretaceous radiolarian biochronology and carbon isotope (Northwestern Pacific, Nadezhda Basin). Proc. Ocean Drill. Program, Sci. Results 185.

Bau, M., Koschinsky, A., 2009. Oxidative scavenging of cerium on hydrous Fe oxide: evidence from the distribution of rare earth elements and yttrium between Fe oxides and Mn oxides in hydrogenetic ferromanganese crusts. Geochem. J. 43, 37–47.

Chester, F.M., Mori, J., Eguchi, N., Toczko, S., Expedition 343/343T Scientists, 2012. Expedition reports Japan Trench Fast Drilling Project (JFAST). Proc. Integr. Ocean Drill. Program, Prelim. Rep. 343–343T.

Chester, F.M., Rowe, C., Ujiie, K., Kirkpatrick, J., Regalla, C., Remitti, F., Moore, J.C., Toy, V., Wolfson-Schwehr, M., Bose, S., Kameda, J., Mori, J.J., Brodsky, E.E., Eguchi, N., Toczko, S., Expedition 343/343T Scientists, 2013. Structure and composition of the plate-boundary slip zone for the 2011 Tohoku-Oki earthquake. Science 342, 1208–1211.

De Baar, H.J.W., Bacon, M.P., Brewer, P.G., 1983. Rare-earth distributions with a positive Ce anomaly in the Western North Atlantic Ocean. Nature 301, 324–327.

Doyle, P.S., Riedel, W.R., 1980. Ichthyoliths from Site 436, Northwest Pacific, Leg 56. Deep Sea Drilling Project.

Faulkner, D.R., Mitchell, T.M., Behnsen, J., Hirose, T., Shimamoto, T., 2011. Stuck in the mud? Earthquake nucleation and propagation through accretionary forearcs. Geophys. Res. Lett. 38, L18303. http://dx.doi.org/10.1029/2011GL048552.

Fujii, Y., Satake, K., Sakai, S., Shinohara, M., Kanazawa, T., 2011. Tsunami source of the 2011 off the Pacific coast of Tohoku Earthquake. Earth Planets Space 63, 815–820.

Fujiwara, T., Kodaira, S., No, T., Kaiho, Y., Takahashi, N., Kaneda, Y., 2011. The 2011 Tohoku-Oki earthquake: displacement reaching the trench axis. Science 334, 1240.

Fulton, P.M., Brodsky, E.E., Kano, Y., Mori, J., Chester, F., Ishikawa, T., Harris, R.N., Lin, W., Eguchi, N., Toczko, S., 2013. Low coseismic friction on the Tohoku-Oki fault determined from temperature measurements. Science 342, 1214–1217.

Ide, S., Baltay, A., Beroza, G.C., 2011. Shallow dynamic overshoot and energetic deep rupture in the 2011 Mw 9.0 Tohoku-Oki earthquake. Science 332, 1426–1429.

Ikari, M.J., Kameda, J., Saffer, D.M., Kopf, A.J., 2015. Strength characteristics of Japan Trench borehole samples in the high-slip region of the 2011 Tohoku-Oki earthquake. Earth Planet. Sci. Lett. 412, 35–41.

Ishikawa, T., Tanimizu, M., Nagaishi, K., Matsuoka, J., Tadai, O., Sakaguchi, M., Hirono, T., Mishima, T., Tanikawa, W., Lin, W., Kikuta, H., Soh, W., Song, S.-R., 2008. Coseismic fluid–rock interactions at high temperatures in the Chelungpu fault. Nat. Geosci. 1, 679–683.

Ito, Y., Tsuji, T., Osada, Y., Kido, M., Inazu, D., Hayashi, Y., Tsushima, H., Hino, R., Fujimoto, H., 2011. Frontal wedge deformation near the source region of the 2011 Tohoku-Oki earthquake. Geophys. Res. Lett. 38, L00G05. http://dx.doi.org/10.1029/2011GL048355.

Kameda, J., Shimizu, M., Ujiie, K., Hirose, T., Ikari, M., Mori, J., Oohashi, K., Kimura, G., 2015. Pelagic smectite as an important factor in tsunamigenic slip along the Japan Trench. Geology 43, 155–158.

Kirkpatrick, J.D., Rowe, C.D., Ujiie, K., Moore, J.C., Regalla, C., Remitti, F., Toy, V., Wolfson-Schwehr, M., Kameda, J., Bose, S., Chester, F.M., 2015. Structure and lithology of the Japan Trench subduction plate boundary fault. Tectonics 34, 53–69. http://dx.doi.org/10.1002/2014TC003695.

Kodaira, S., No, T., Nakamura, Y., Fujiwara, T., Kaiho, Y., Miura, S., Takahashi, N., Kaneda, Y., Taira, A., 2012. Coseismic fault rupture at the trench axis during the 2011 Tohoku-Oki earthquake. Nat. Geosci. 5, 646–650.

Koper, K.D., Hutko, A.R., Lay, T., Ammon, C.J., Kanamori, H., 2011. Frequency-dependent rupture process of the 2011 Mw 9.0 Tohoku Earthquake: comparison of short-period P wave backprojection images and broadband seismic rupture models. Earth Planets Space 63, 599–602.

Labaume, P., Maltman, A.J., Bolton, A., Tessier, D., Ogawa, Y., Takizawa, S., 1997. Scaly fabrics in sheared clays from the décollement zone of the Barbados accretionary prism. Proc. Ocean Drill. Program, Sci. Results 156.

Langseth, M., Okada, H., Adelseck, C., Bruns, T., Harper, H.E., Kurnosov, V., Muller, G., Murdmaa, I., Pisciotto, K.A., Robinson, P., Sakai, T., Thompson, P.R., Whelan, J., Wories, H., 1977. Site 436: Japan Trench Outer Rise, Leg 56. Proceedings of the Deep Sea Drilling Project Preliminary Report.

Lin, W., Fulton, P.M., Harris, R.N., Tadai, O., Matsubayashi, O., Tanikawa, W., Kinoshita, M., 2014. Thermal conductivities, thermal diffusivities, and volumetric heat capacities of core samples obtained from the Japan Trench Fast Drilling Project (JFAST). Earth Planets Space 66, 48.

Maltman, A., Labaume, P., Housen, B., 1997. Structural geology of the décollement at the toe of the Barbados accretionary prism. Proc. Ocean Drill. Program, Sci. Results 156.

Minoura, K., Imamura, F., Sugawara, D., Kono, Y., Iwashita, T., 2001. The 869 Jogan tsunami deposit and recurrence interval of large-scale tsunami on the Pacific coast of northeast Japan. J. Nat. Disaster Sci. 23, 83–88.

Moore, G.F., Shipley, T.H., Stoffa, P.L., Karig, D.E., Taira, A., Kuramoto, S., Tokuyama, H., Suyehiro, K., 1990. Structure of the Nankai trough accretionary zone from multichannel seismic reflection data. J. Geophys. Res. 95, 8753–8765.

Moore, J.C., Plank, T.A., Chester, F.M., Polissar, P.J., Savage, H.M., 2015. Sediment provenance and controls on slip propagation: lessons learned from the 2011 Tohoku and other great earthquakes of the subducting northwest Pacific plate. Geosphere 11, 3. http://dx.doi.org/10.1130/GES01099.1.

Moore, J.C., Roeske, S., Cowan, D.S., Lundberg, N., Gonzales, E., Lucas, S.E., Schoonmaker, J., 1986. Scaly fabrics from Deep Sea Drilling Project cores from forearcs. In: Geological Society of America Memoirs, vol. 166, pp. 55–74.

Nakamura, Y., Kodaira, S., Miura, S., Regalla, C., Takahashi, N., 2013. High-resolution seismic imaging in the Japan Trench axis area off Miyagi, northeastern Japan. Geophys. Res. Lett. 40, 1713–1718.

Plank, T., 2014. The chemical composition of subducting sediments. In: Holland, H.D., Turekian, K.K. (Eds.), Treatise on Geochemistry. Elsevier Ltd., Oxford, pp. 607–629.

Plank, T., Kelley, K.A., Murray, R.W., Stern, L.Q., 2007. Chemical composition of sediments subducting at the Izu–Bonin trench. Geochem. Geophys. Geosyst. 8, Q04I16. http://dx.doi.org/10.1029/2006GC001444.

Plank, T., Langmuir, C.H., 1998. The chemical composition of subducting sediment and its consequences for the crust and mantle. Chem. Geol. 145, 325–394.

Plank, T., Ludden, J.N., Escutia, C., Party, S.S., 2000. 1. Leg 185 summary: inputs to the Izu–Mariana subduction system. Proc. Ocean Drill. Program, Initial Rep. 185.

Poliakov, A.N.B., Dmowska, R., Rice, J.R., 2002. Dynamic shear rupture interactions with fault bends and off-axis secondary faulting. J. Geophys. Res. 107, B11.

Rowe, C.D., Moore, J.C., Remitti, F., Scientists, E., 2013. The thickness of subduction plate boundary faults from the seafloor into the seismogenic zone. Geology 41, 991–994.

Sawai, M., Hirose, T., Kameda, J., 2014. Frictional properties of incoming pelagic sediments at the Japan Trench: implications for large slip at a shallow plate boundary during the 2011 Tohoku earthquake. Earth Planets Space 66, 65.

Sawai, Y., Namegaya, Y., Okamura, Y., Satake, K., Shishikura, M., 2012. Challenges of anticipating the 2011 Tohoku earthquake and tsunami using coastal geology. Geophys. Res. Lett. 39, L21309. http://dx.doi.org/10.1029/2012GL053692.

Simons, M., Minson, S.E., Sladen, A., Ortega, F., Jiang, J., Owen, S.E., Meng, L., Ampuero, J.P., Wei, S., Chu, R., Helmberger, D.V., Kanamori, H., Hetland, E., Moore, A.W., Webb, F.H., 2011. The 2011 magnitude 9.0 Tohoku-Oki earthquake: mosaicking the megathrust from seconds to centuries. Science 332, 1421–1425.

Tanikawa, W., Hirose, T., Mukoyoshi, H., Tadai, O., Lin, W., 2013. Fluid transport properties in sediments and their role in large slip near the surface of the plate boundary fault in the Japan Trench. Earth Planet. Sci. Lett. 382, 150–160.

Ujiie, K., Kimura, G., 2014. Earthquake faulting in subduction zones: insights from fault rocks in accretionary prisms. Prog. Earth Planet. Sci. 1 (7).

Ujiie, K., Tanaka, H., Saito, T., Tsutsumi, A., Mori, J.J., Kameda, J., Brodsky, E.E., Chester, F.M., Eguchi, N., Toczko, S., 2013. Low coseismic shear stress on the Tohoku-Oki megathrust determined from laboratory experiments. Science 342, 1211–1214.

Vannucchi, P., Maltman, A., Bettelli, G., Clennell, B., 2003. On the nature of scaly fabric and scaly clay. J. Struct. Geol. 25, 673–688.

Wade, J.A., Plank, T., Stern, R.J., Tollstrup, D.L., Gill, J.B., O'Leary, J.C., Eiler, J.M., Moore, R.B., Woodhead, J.D., Trusdell, F., Fischer, T.P., Hilton, D.R., 2005. The May 2003 eruption of Anatahan volcano, Mariana Islands: geochemical evolution of a silicic island-arc volcano. J. Volcanol. Geotherm. Res. 146, 139–170.

Yang, T., Mishima, T., Ujiie, K., Chester, F.M., Mori, J.J., Eguchi, N., Toczko, S., 2013. Strain decoupling across the décollement in the region of large slip during the 2011 Tohoku-Oki earthquake from anisotropy of magnetic susceptibility. Earth Planet. Sci. Lett. 381, 31–38.